

# **Topographic experiments over dynamical processes in the Norwegian Sea**

*Tatyana V. Belonenko<sup>1</sup>, Vladimir S. Travkin<sup>1</sup>,  
Aleksey V. Koldunov<sup>1</sup>, Denis L. Volkov<sup>2,3</sup>*

<sup>1</sup>Saint Petersburg State University, Saint Petersburg, Russia

<sup>2</sup>Cooperative Institute for Marine and Atmospheric Studies,  
University of Miami, Miami, FL, USA

<sup>3</sup>Atlantic Oceanographic and Meteorological Laboratory,  
NOAA, Miami, FL, USA

**Abstract.** The Norwegian Atlantic Current is significantly steered by large topographic features of the Norwegian Sea. The geometry of topographic features in the region is highly variable, but the influence of this variation on the formation of a quasi-permanent anticyclonic vortex located in the center of the Lofoten Basin (Lofoten Vortex) is poorly understood. Four sensitivity experiments with a regional configuration of the Massachusetts Institute of Technology general circulation model have been carried out with an objective to investigate the role of bottom topography on the formation of the Lofoten Vortex in the Norwegian Sea. We find that the bottom topography and especially the geometry of subsurface ridges are critical for the dynamics of the Norwegian Sea and stability of the Lofoten Vortex.

# 1. Introduction

The bottom topography has an important influence on ocean circulation, especially in high-latitude basins, such as the Norwegian Sea. Due to the conservation of potential vorticity in a spinning ocean

$$\frac{D}{Dt} \left( \frac{f + \zeta}{H} \right) = 0$$

where the planetary vorticity  $f$  tends to be much larger than relative vorticity  $\zeta$ ,  $f/H$  becomes nearly constant, i.e. barotropic flows follow the  $f/H$  contours. Because the gradient of planetary vorticity at high latitudes is small, bottom topography becomes the dominant component of the  $f/H$  field, so that the large-scale circulation here tend to follow the contours of constant depth [*Isachsen*, 2003; *Nøst and Isachsen*, 2003]. The importance of topographic steering in the Nordic Seas has been confirmed by observations with surface drifters, Argo and RAFOS floats [*Bosse et al.*, 2019; *Dugstad et al.*, 2019; *Gascard and Mork*, 2008; *Jakobsen et al.*, 2003; *Koszalka et al.*, 2011; *Orvik and Nøller*, 2002; *Poulain et al.*, 1996; *Rossby et al.*, 2009; *Voet et al.*, 2010].

The Norwegian Sea consists of two basins, the Nor-

wegian Basin (NB) in the south and the Lofoten Basin (LB) in the north, separated from each other by the Vøring Plateau and the Helgeland Ridge (Figure 1). These topographic boundaries make the basins relatively isolated with distinct dynamic and thermohaline characteristics. The LB represents a bowl-shaped topographic depression with a maximum depth of about 3250 m, while the NB features greater depths (up to 4000 m) and a rather rough seafloor, complicated by sea mountains. The Norwegian Sea is an important transit region for the warm and salty Atlantic Water on its way to the Arctic Ocean. The circulation of the Norwegian Sea is dominated by the Norwegian Atlantic Current (NwAC), which forms three main branches: the Norwegian Atlantic Slope Current (NwASC), the Norwegian Atlantic Front Current (NwAFC), and Norwegian Coastal Current (NCC). The main characteristic of the LB, which makes it different from the NB, is a local maximum of mesoscale activity and significant heat exchange with the atmosphere [*Belonenko et al., 2014; Fer et al., 2018; Gordeeva et al., 2020; Volkov et al., 2013*].

Mesoscale eddies are mainly generated through the instability of the NwASC and propagate towards the central part of the LB [*Köhl, 2007; Raj and Halo, 2016*;

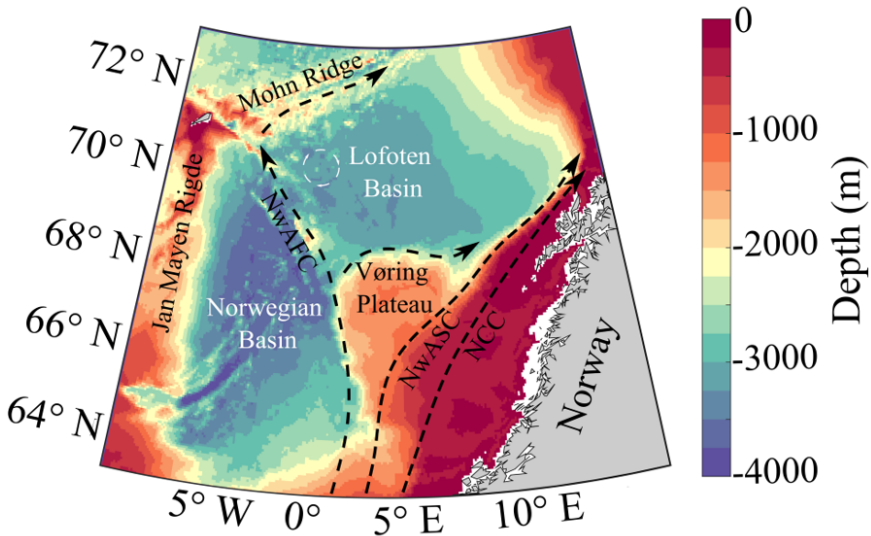


**Figure 1.** The study area. The color indicates bottom topography (m). The arrows indicate the main currents. NwAFC – Norwegian Frontal Current, NwASC – Norwegian Slope Current, and NCC – Norwegian Coastal Current. The white circle marks the location of the quasi-permanent anticyclonic Lofoten Vortex.

*Volkov et al.*, 2013, 2015]. They transport heat and salt from the periphery to the central part of the domain (see estimations in [*Belonenko et al.*, 2020]). A shape of the LB like a deep bowl and monotone increasing of depth towards the center leads to increasing the thickness of the Atlantic Water layer in the center of the LB, whereby the speed of water transfer northwards

falls there [Rossby et al., 2009]. Orvik [2004] indicated that strong penetration of the Atlantic Waters in the LB is manifested exactly by low velocities and the corresponding reduced water transfer northward. This determines why the LB differs from the NB, which is only half-filled with the Atlantic Waters.

The most important feature of the LB is a quasi-permanent anticyclonic Lofoten vortex (LV) located over the deepest part of the basin [Alekseev et al., 1991; Belonenko et al., 2018; Ivanov and Korablev, 1995a, 1995b; Rossby et al., 2009]. The main body of the LV is confined to the depths of 300–1000 m, however, there are indications that the dynamic signal of the vortex can reach the bottom (e.g. [Volkov et al., 2015]). Based on observations with Seagliders, collected between July 2012 and July 2015, Yu et al. [2017] estimated the dynamical radius of the Lofoten Vortex core equals  $18 \pm 4$  km and the maximum orbital velocities  $50\text{--}70 \text{ cm s}^{-1}$ . Bashmachnikov et al. [2017b] estimated the dynamical radius of the Lofoten Vortex as 30 km. Ivanov and Korablev [1995a] and Søiland et al. [2016] describe the LV as a convective lens of warm and saline water between 300–1000 m depth with a diameter of up to 100 km (see also [Volkov et al., 2015]).

Because the conservation of potential vorticity fa-

vors cyclonic circulations over topographic depressions in the Northern Hemisphere, the localization of a quasi-permanent anticyclonic eddy in the LB is an interesting and not fully understood oceanographic phenomenon. Nowadays, there are two main points of view on the generation and stability of the LV. The first was initially proposed by *Ivanov and Korablev* [1995a, 1995b]), who showed that deep convection in winter and further summer relaxation could be responsible for the annual regeneration of the LV [see also *Alexeev et al.*, 2016; *Bashmachnikov et al.*, 2017b, 2018; *Belonenko et al.*, 2017; *Bloshkina and Ivanov*, 2016; *Søiland et al.*, 2016]. They claimed that the influence of bottom topography is limited to the formation of a topographically-controlled cyclonic background flow, which keeps the LV within the LB. The second point of view is based on an idea that the LV reinforces mainly due to merges with other mesoscale eddies, generated by the NwAC and propagated to the center of the LB [*Isachsen*, 2011, 2015; *Köhl*, 2007; *Raj et al.*, 2020; *Rossby et al.*, 2009; *Volkov et al.*, 2015]. The combined effect of these two processes in the presence of bottom topography is considered by *Zinchenko et al.* [2019] and *Gordeeva et al.* [2020], who provided the complex statistical analysis of mesoscale eddies in the basin.

Although a number of studies have been dedicated to the dynamics and thermohaline properties of the LV, the role of bottom topography in its formation has not been experimentally assessed. Using idealized numerical experiments with a bowl-shaped basin, *Shchepetkin* [1995] reported that an initially turbulent flow tends to organize in a cyclonic circulation along the periphery of the basin and forms an anticyclonic vortex in its center. Earlier, based on experiments with a rotating tank, *Carnevale et al.* [1991] showed that if the horizontal scale of eddies is smaller than that of the basin, the topographic  $\beta$ -effect attracts anticyclonic eddies downslope in a cyclonic spiral towards the center of a topographic depression, while cyclones tend to move upslope. Thus, the cyclonic propagation of anti-cyclones towards the deepest part of the LB and their subsequent merging can represent a likely mechanism for the existing and stability of the quasi-permanent LV and its positioning over the deepest part of the basin. This hypothesis was well supported by several eddy-permitting and eddy-resolving numerical experiments that provided additional evidence for the importance

of eddies in the formation and regeneration of the LV [Volkov et al., 2015]. The topographical structure of the LB possibly contributes to the fact that the anti-cyclonic LV is stable and does not leave the LB, only moving along a quasi-cyclonic trajectory within it [Belenikov, 2005].

The main goal of this paper is to assess the role of bottom topography in the formation of the LV in the Norwegian Sea. Specifically, we aim to answer the following questions: (i) Why quasi-permanent anticyclonic eddy is generated in the LB but is not generated in the NB? (ii) Would the characteristics of the anticyclonic eddy in the center of the basin differ for different types of bottom topography? (iii) How does mesoscale eddy variability influence the generation of the LV? (iv) How does bottom topography influence the Mixed Layer Depth (MLD) in the Norwegian Sea? (v) Would MLD correlate with mesoscale eddy activity? To answer these questions, we conduct four numerical experiments with modified bottom topography, but realistic lateral boundary conditions and forcing.

## 2. Methods

### 2.1. Numerical Experiments

The numerical experiments are based on a regional configuration of the Massachusetts Institute of Technology general circulation model [MITgcm; *Marshall et al.*, 1997]. The model setup is similar to the one described in *Nguyen et al.* [2011] and *Volkov et al.* [2015]. The regional domain was designed for multi-purpose applications and includes the North Atlantic and the Arctic Ocean (see Figure 2 in [*Volkov et al.*, 2015]). The model has 50 vertical levels with intervals ranging from 10 m at the surface to 456 m at depth. Bathymetry represents a blend of the *Smith and Sandwell* [1997] and the General Bathymetric Charts of the Oceans (GEBCO) one-arc minute bathymetric grid. The model uses partial cell formulation of *Adcroft et al.* [1997], which permits the accurate representation of the bathymetry. Vertical mixing follows the K-profile parameterization (KPP) of *Large et al.* [1994]. The ocean model is coupled with the MITgcm sea-ice model described in *Losch et al.* [2010]. The model is integrated into a volume-conserving configuration using a finite volume discretization with a C-grid

staggering of the prognostic variables. The topography of the seafloor is based on a digital bathymetric map of the World Ocean (GEBCO) with a spatial resolution of 1 mile. To assess the influence of topography on the intensity of deep convection, numerical experiments were performed: TOPO1, TOPO2, TOPO3 and TOPO4 with different variants of the topography of the Norwegian Sea (Figure 2). The TOPO1 experiment has a realistic bottom topography. In the TOPO2 experiment, the periphery of the Lofoten and Norwegian Basins is made flat with a depth of 3000 m except for some parts of Jan Mayen and Mohn Ridges as well as the continental slope of Norway. There is no Vøring Plateau and no Helgeland Ridge (Figure 2). The topography of the TOPO3 experiment (Figure 2) is similar to that of TOPO2 for the NB, but there is no topographic depression in the area of the LB. The bottom topography of the NB is represented by a flatter area compared to TOPO2 since sea mountains and ridges in the NB are removed and the bottom is made flat with a depth of 3500 m. In the TOPO4, the bottom topography in the LB is represented by a flat bottom with a depth of 2500 m without the Helgeland Ridge, while the bottom topography in the NB is realistic (Figure 2).

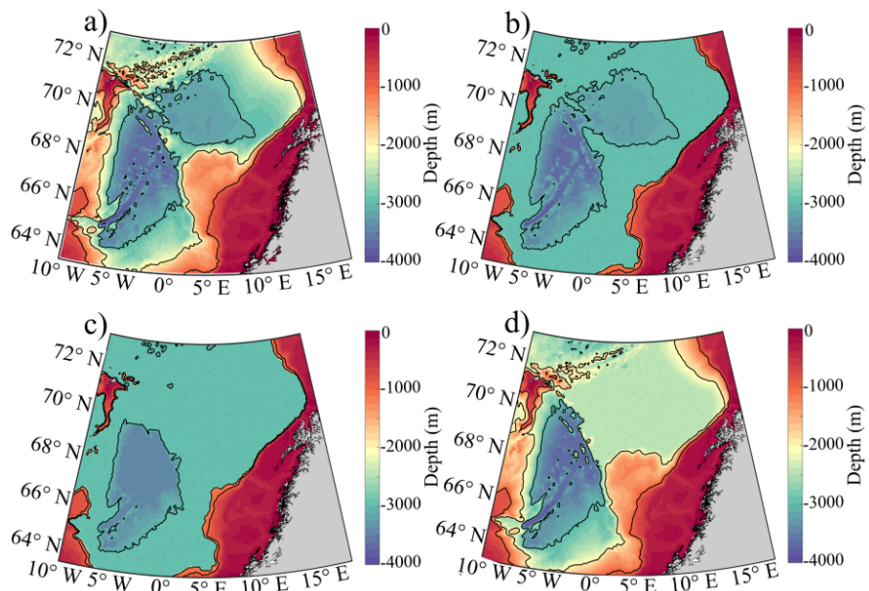


**Figure 2.** Bottom topography for topographical experiments. Isobath carried out after every 1000 m.

## 2.2. Mixed Layer Depth Evaluation

The area of the Norwegian Sea is known as a region of deep winter convection [*Fedorov et al.*, 2019; *Köhl*, 2007; *Nilsen and Falck*, 2006; *Travkin and Belonenko*, 2020]. *Köhl* [2007] using the MITgcm showed that deep convection in the winter of 1997–2004 in the area of the LV exceeds depths of 1000 m. Similar estimates of MLD were obtained by *Alexeev et al.* [2016], where

the authors relied on data from field surveys. Using the MITgcm and Argo data, *Fedorov et al.* [2018, 2019] obtained an estimate of MLD reaching 1000 m for the period 1993–2012.

To estimate MLD in this study, we used the method of Kara [*Kara et al.*, 2000]. The MLD is defined as a depth of the horizon at which the water density changes by a certain value compared to the sea surface. An empirical criterion of the density change in this method is defined as the difference between the water density with temperature  $T_r$  and salinity  $S$  at the sea surface  $r$  (or 10 m) and the density with the same salinity  $S$  and temperature  $T_h$ :

$$\Delta\sigma = \sigma(T_r, S) - \sigma(T_h, S).$$

*Kara et al.* [2000] indicated that one must carefully choose a criterion for determining the MLD, taking into account hydrological conditions in the study area. We use the temperature criterion (difference) equal to  $0.1^{\circ}\text{C}$ , so that  $T_h = T_r - 0.1$ . The reason for the criterion is given in the Supplement **747-s01.png**. The horizon, where the density difference exceeds  $\Delta\sigma$ , is considered as MLD. This method takes into account the nonlinearity of the equation of state since the value

of the criterion depends on the salinity and temperature.

## 3. Results

### 3.1. The Time-Mean Circulation in the Norwegian Sea

Streamlines, constructed using the mean velocities at 95 m depth (Figure 3), show the main structures of the large-scale circulation in the TOPO experiments. As expected, the main currents in the experiments tend to follow isobaths. Clearly, the absence of the Vøring Plateau in the experiments TOPO2 and TOPO3 has a strong impact on the circulation. The absence of the boundary between the basins is favorable for unobstructed water exchange between them. The anticyclonic LV is generated in TOPO1 and TOPO2, but it does not form in TOPO3 and TOPO4. The size of the vortex in TOPO2 is somewhat larger than in TOPO1 (Supplement **747-fra.mp4**). Interestingly, while the LV does not form in the LB in TOPO3, a quasi-permanent anticyclonic vortex forms over the deepest part of the NB instead (Figure 3). It should be remembered that in TOPO3 we smoothed the bottom of the NB

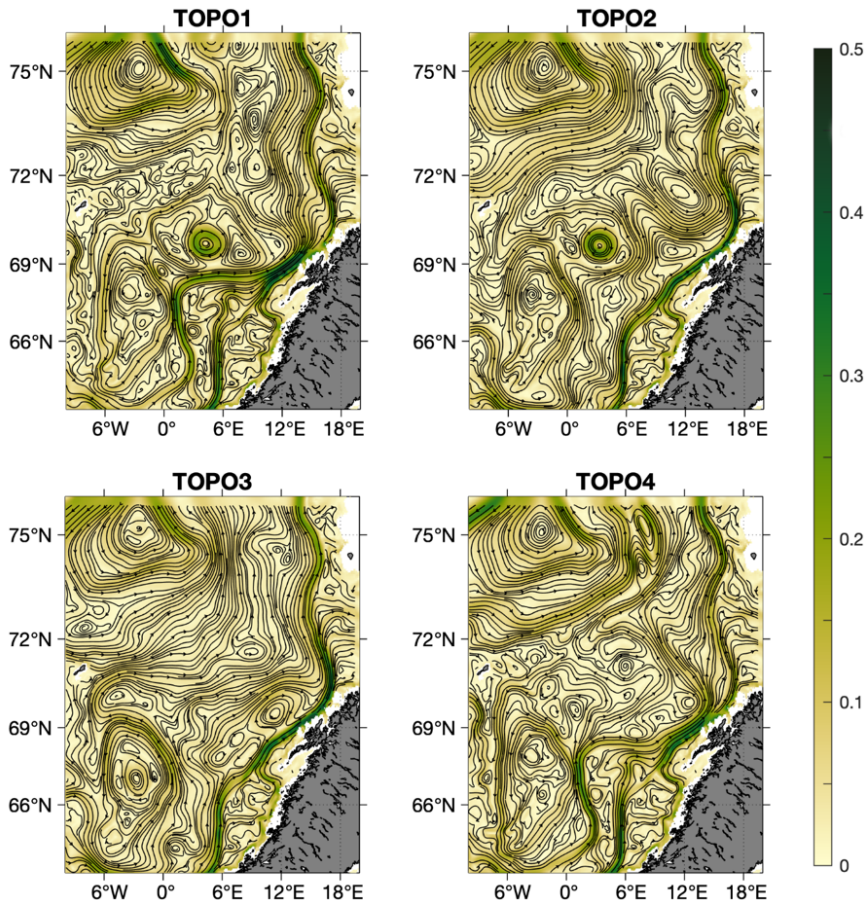


**Figure 3.** Time-mean spatial distribution of velocities,  $\text{m s}^{-1}$  (shown in color) and the corresponding streamlines the 95 m layer.

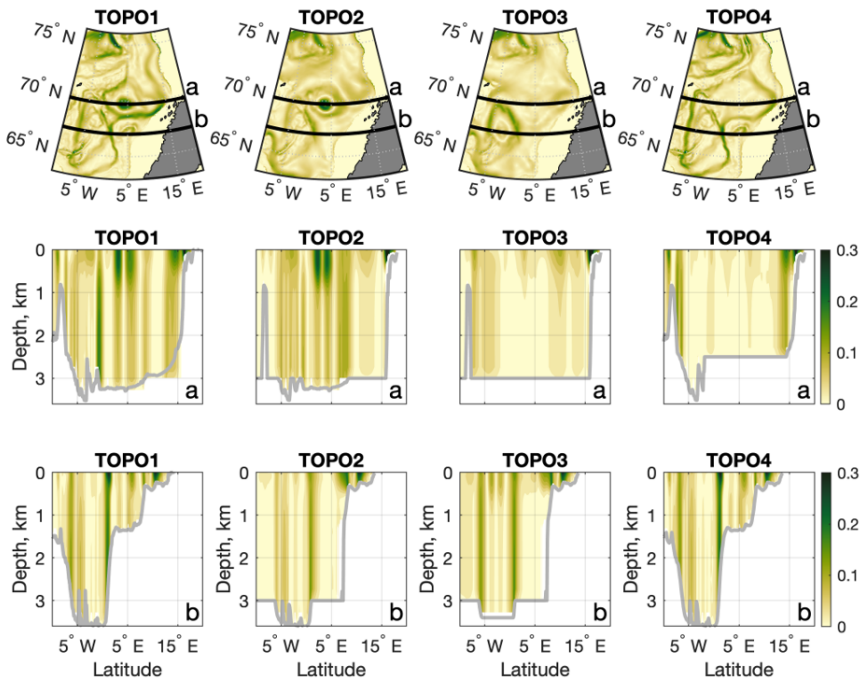


**Figure 4.** Mean velocity fields at the 500 m horizon (top) and vertical cross-sections of velocities along  $69.72^{\circ}\text{N}$  (a) and  $67.02^{\circ}\text{N}$  (b) in the TOPO experiments.

by removing sea mountains and ridges. In TOPO4, in which the bottom of the NB is made realistic, an anticyclonic vortex in the NB does not form. Thus, it is clear that favorable bottom topography represents a necessary condition for the formation of a quasi-permanent vortex in the center of a topographic depression. The anticyclonic vortex formed in TOPO3 has a comparable size and intensity to the LV in the NB in TOPO1.

### **3.2. Vertical Cross-Sections in the Norwegian Sea**

Since the quasi-permanent vortex in the Norwegian Sea is the main focus of this paper, we consider two vertical cross-sections. The first goes along  $69.72^{\circ}\text{N}$  and crosses the center of the LV in the LB (see Figure 3 for TOPO1). The second stretches along  $67.02^{\circ}\text{N}$  and crosses the center of the quasi-permanent vortex generated in TOPO3 in the NB (see Figure 3 for TOPO3). Figure 4 shows that maximum velocities in the LB are observed in the area of the LV (see Figure 4 for TOPO1 and TOPO2). Increased velocities associated with the LV can be traced to the bottom, but maximum velocities are concentrated within the core of the vortex in the upper 1000 m. TOPO1 also features a strong branch

of the NwAFC. Note that large velocities in the NwAFC are seen to the bottom (3250 m). This feature does not exist in the TOPO2 experiment where the NwAFC is much weaker. TOPO1 also demonstrates the stronger NwASC although maximum velocities are only visible in the upper 500 m, which is much less than in TOPO2. Velocities in TOPO3 are small except near the Scandinavian coast with relatively strong velocities in the upper 500 m. In TOPO4, one can see an enhancement of the meridional flows near the periphery and weak velocities in the center of the LB.

The averaged fields and cross-sections of temperature (Figure 5) and salinity (Supplement **747-s02.png**) illustrate the distribution of warm and salty water westward from the branch of the NwASC. The vertical extent of the LV in TOPO1 and TOPO2 exceeds 1300 m while the vortex in the NB has less depth visible in temperature and salinity characteristics. In TOPO3, the vortex in the center of the NB forms with temperature and salinity anomalies 1100 m. In TOPO4, the vortex does not form in any of the basins.

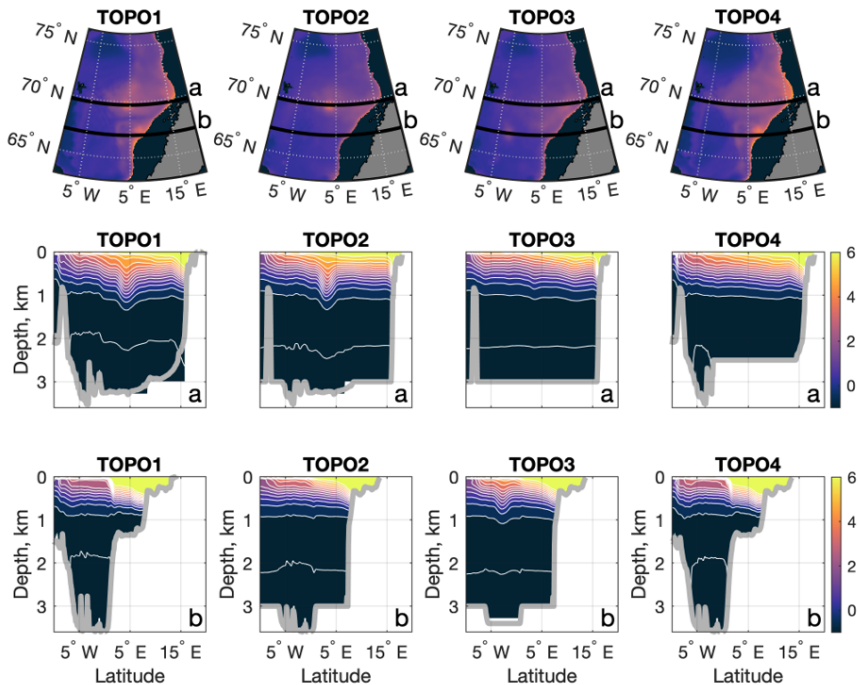


**Figure 5.** Temperature at the 500 m horizon (top) and vertical cross-sections of temperature along  $69.72^{\circ}\text{N}$  (a) and  $67.02^{\circ}\text{N}$  (b) in the TOPO experiments.

### 3.3. Vorticity Maps and Generation of an Anticyclonic Vortex in the TOPO Experiments

In the experiment TOPO1 (Supplement **747-t01.mp4**), a topographic vortex in the center of the LB is formed within six months after the beginning of the simulation of MITgcm. In July 1992, a large anticyclone is observed in the center of the LB around  $69.8^{\circ}\text{N}$ ,  $5.9^{\circ}\text{E}$ . This vortex moved subsequently within the basin and existed until the end of the experiment (Figure 6). It is important to note that several large anticyclonic vortices can be observed simultaneously at any given time in TOPO1. (Figure 6) shows that these vortices are confined to the areas of the main currents in the region since they are formed due to their barotropic and baroclinic instability. Previous studies indicate a quasi-cyclonic movement of the LV in the LB [e.g. *Alexeev et al.*, 2016; *Bloshkina and Ivanov*, 2016; *Ivanov and Korablev*, 1995b; *Volkov et al.*, 2015].

In TOPO2 (Supplement **747-t02.mp4**), the generation of the LV occurs a month earlier than in TOPO1. Analysis of vorticity maps shows that the concentration of anticyclonic vorticity in the center of the basin is absent in May 1992, but it is formed by 17 June 1992 and exists until the end of the experiment. Despite the bottom topography in TOPO2 corresponds to TOPO1 at

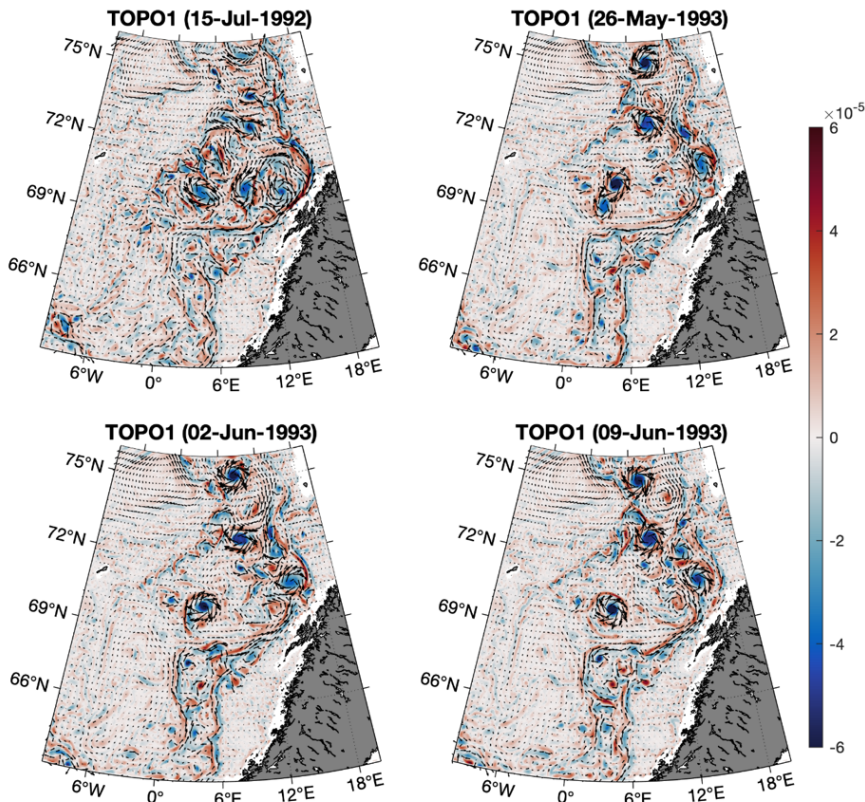


**Figure 6.** Relative vorticity (color) and velocities (arrows) at the 95 m horizon in TOPO1.

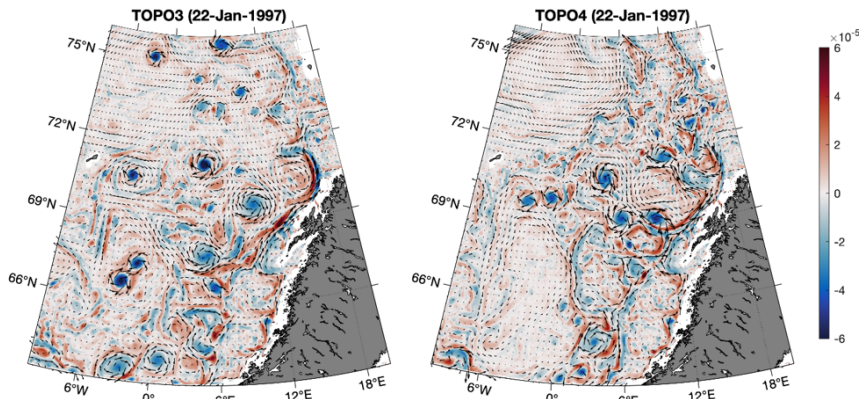


**Figure 7.** Relative vorticity (color) and velocities (arrows) at the 95 m horizon in TOPO3 and TOPO4.

depths greater than 3000 m, there is no smooth change in depth in TOPO2 since the values of the bottom topography  $H$  in the range from  $1000 < H < 3000$  m are replaced with values of 3000 m. Perhaps this is what leads to faster formation of the LV in TOPO2 in comparison to TOPO1.

While mesoscale variability in TOPO3 is present in both the LB and the NB (Supplement **747-t03.mp4**), no quasi-permanent vortex is formed in the LB. The absence of topographic obstacles between the basins allows the anticyclones formed in the LB enter the NB and get entrained in the basin's cyclonic circulation following the  $f/H$  contours (Figure 7).

The experiment TOPO4 (Supplement 747-t04.mp4) shows the significant role the bottom topography plays and, in particular, the topographic boundary separating the Norwegian sea into two basins. The Helgeland Ridge and the Vøring Plateau divide the Norwegian Sea into two basins. When the Helgeland Ridge and the Vøring Plateau are excluded from the analysis, the Norwegian Sea is a single area, where there are various types of mesoscale activity in the whole domain. Unlike TOPO3, the boundary between the basins exists in TOPO2 and TOPO4, and mesoscale activity in the LB is rich and almost absent in the NB (Figure 7). It seems that the smooth bottom topography and lack of seamounts and ridges are the most important for the generation of the quasi-permanent vortex in the NB. The period of the quasi-permanent anticyclone generation in the Norwegian Sea is different for two basins (see Table 1).

### **3.4. Winter Convection in the Norwegian Sea in the TOPO Experiments**

Figure 8 shows the time series of the spatially averaged values of MLD in the TOPO experiments for 1993 to 1997. We found out that the MLD in the LB exceeds

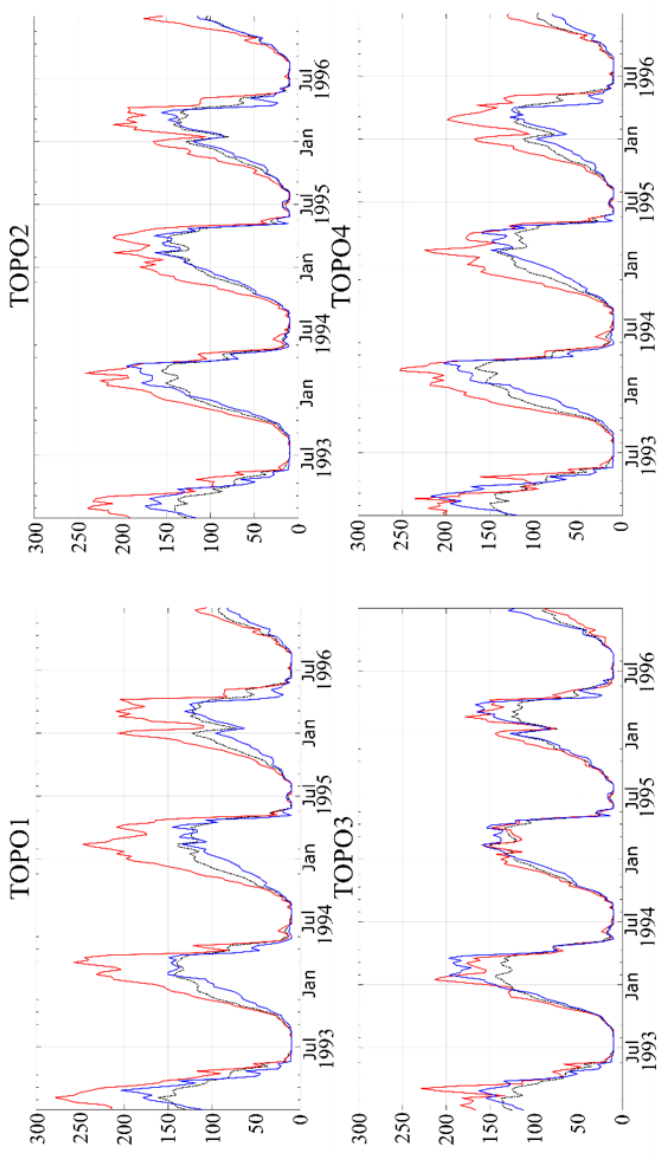


**Figure 8.** Temporal variability of MLD averaged for the area of the LB (red), NB (blue), and Norwegian Sea (black) in the TOPO experiments.

**Table 1.** The Time (in Months) Necessary for the Generation of the Quasi-Permanent Anticyclone in the Center of the Basins

	LB	NB
TOPO1	6.5	is not generated
TOPO2	5.5	is not generated
TOPO3	is not generated	22
TOPO4	is not generated	14

the MLD in the NB in TOPO1, TOPO2, and TOPO4, while in TOPO3, the similar values of the MLD are observed in both basins. This similarity in the TOPO3 is due to the lack of topographic boundaries between the basins wherein in the TOPO3 experiment, mesoscale eddies accumulate in the NB and favor the development of deep convection in the spring-winter period. It is the presence of a quasi-stationary vortex with deep convection and turbulent mixing that increases the MLD in this area.

In December and January, the average values of MLD for the TOPO experiments do not exceed 125 m, but in February they become bigger and reach their maximum (Figure 9). Then, MLD slightly decreases in March, while in April the process of deep convection almost

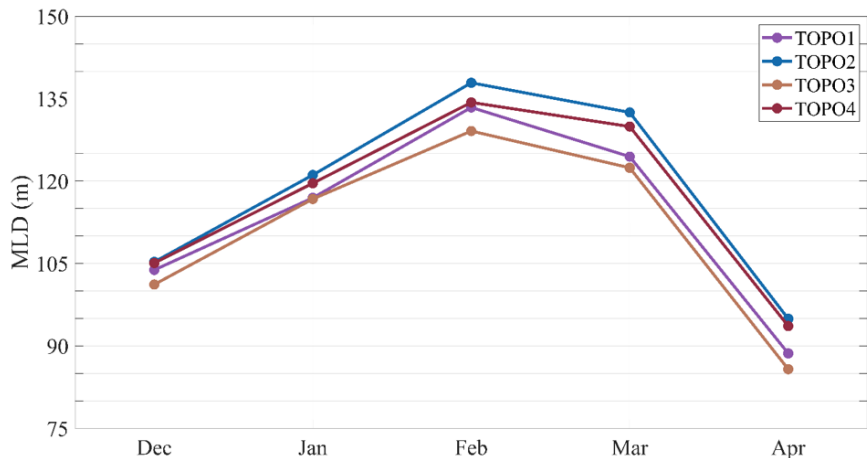


**Figure 9.** Seasonal variability of the mean values of MLD from 1993–1997 for the TOPO experiments.

stops, which leads to a decrease of MLD lower than in December. The highest values of MLD in February and March are observed in TOPO2 while the lowest is observed in the TOPO3 experiment.

Deep convection is one of the main reasons for the annual regeneration of quasi-permanent vortex and its stability [*Ivanov and Korablev*, 1995a]. The spatial distributions of MLD in the TOPO experiments show the maximum values in the locations of the quasi-permanent vortex (Figure 10). The same results were obtained by *Nilsen and Falck* [2006] and *Fedorov et al.* [2019], where in situ, model, and satellite data were used for

calculations of MLD. Figure 10 shows that the values of MLD in the LB exceed 400 m in the area of the LV location. In the TOPO3 experiment, the maxima of MLD are located in the NB and correspond to the location of the quasi-permanent vortex. In the TOPO4, the maxima of MLD are distributed across the LB and Vøring Plateau as well. Notice that the Vøring Plateau exists only in the TOPO1 and TOPO4, and there are significant values of MLD in the Vøring Plateau in these experiments.

### 3.5. Eddy Kinetic Energy in the TOPO Experiments

Eddy Kinetic Energy (EKE) is calculated based on horizontal fluctuations in the flow rate ( $u'$  and  $v'$ ):

$$EKE = \frac{u'^2 + v'^2}{2},$$

here  $u'$  and  $v'$  are the anomalies of the flow components  $u$  and  $v$  relative to their average values in each cell of the grid net for 1993 to 1997. In the TOPO1 experiment, the maximum EKE reaching about  $600 \text{ cm}^2 \text{ s}^{-2}$  is observed in the central part of the LB and near the continental slope of Norway (Figure 11). Large EKE

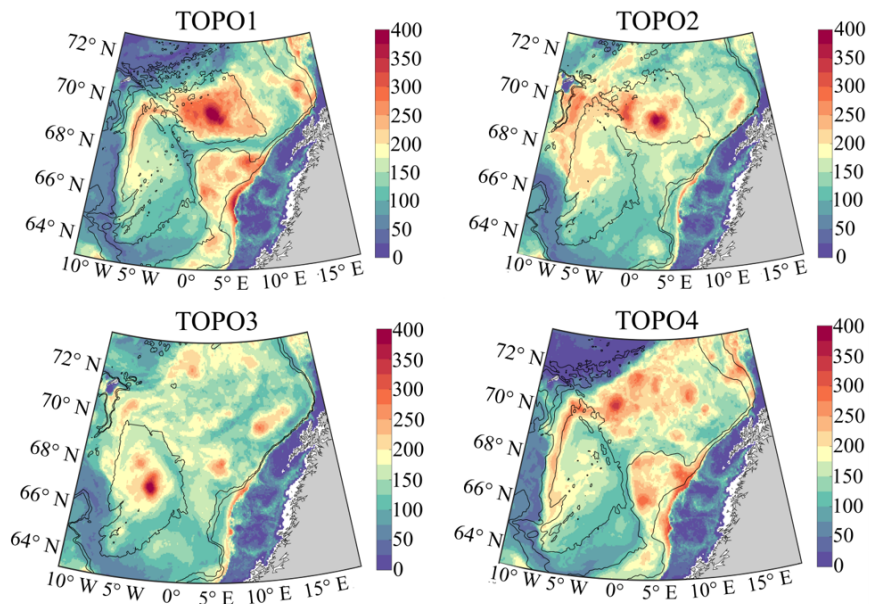


**Figure 10.** Spatial distribution of MLD (m) in February averaged for 1993–1997 in the TOPO experiments.

values of up to  $300 \text{ cm}^2 \text{ s}^{-2}$  are also seen over the Vøring Plateau, while in the NB EKE is very small and does not exceed  $50 \text{ cm}^2 \text{ s}^{-2}$ . In the TOPO2 experiment, there is an increase of eddy activity over the Norwegian continental slope, especially in the southern part of the Norwegian Sea (Figure 11), and there is also a slight increase along the boundaries of the NB, and in the western parts of the LB and NB. In the

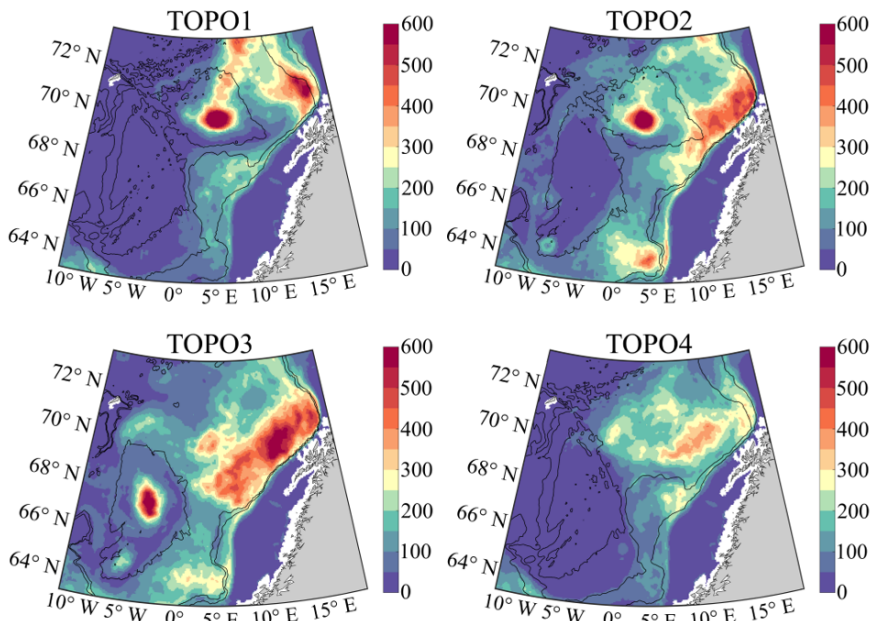


**Figure 11.** Spatial distribution of EKE ( $\text{cm}^2 \text{ s}^{-2}$ ) in February averaged for 1993–1997 in the TOPO experiments.

TOPO3 experiment, the maximum EKE is observed in the eastern part of the LB along the continental slope and in the central part of the NB (Figure 11). In the central part of the LB, the EKE values are smaller than in TOPO1 and TOPO2. In the TOPO4 experiment, there are no EKE values greater than  $400 \text{ cm}^2 \text{ s}^{-2}$  in the LB, and there is a shift in the area of the highest values of EKE to the eastern part of the LB. Based on

the numerical experiments, it is possible to conclude that the topographic depression in the LB and the topographic boundary with the adjacent NB in TOPO1 and TOPO2 lead to the concentration of EKE in the LB and to small EKE in the NB. If there is no boundary between the basins, eddies freely enter the NB and form a quasi-permanent anticyclonic vortex, associated with high EKE in the center of the basin. However, when the boundaries in the form of the Voring Plateau and the Helgeland Ridge are restored in TOPO4, the vortex does not form and EKE in the center of the NB is very small as in TOPO1 and TOPO2. Thus, the TOPO experiments show that bottom topography plays a crucial role in the localization of mesoscale eddy activity in the Norwegian Sea.

### **3.6. Eddy and Slope Convection (Linkage of EKE to MLD in the TOPO Experiments)**

Comparison of Figure 10 and Figure 11 shows that the regions of maximum MLD mostly coincide with the regions of maximum EKE. Vertical vortex mixing contributes to the strengthening of convective processes, so the maximum values of MLD in the Norwegian Sea are located in vortices with maximums of EKE. In the

TOPO1 experiment, the maximum values of MLD exceeding 400 m are located in the LV area with a maximum of EKE of  $600 \text{ cm}^2 \text{ s}^{-2}$ . Figure 10 also shows the increased values of MLD in the north-eastern part of the LB near the Scandinavian slope. These local maxima correspond to the increased values of EKE in Figure 11. There is also some correlation over the Vørting Plateau. However, there are also differences, e.g. in Figure 10, the MLD up to 300 m is not accompanied by an increase in EKE along the Mohn Ridge in the NB. This suggests that other types of vertical mixing not associated with eddies, and this is the slope convection. Slope convection can exist simultaneously with convection in eddies, and this leads to the fact that the areas of increased values of MLD are significantly larger than the areas with increased values of EKE (see Figure 10 and Figure 11).

In TOPO2, the spatial location of the main maxima of MLD and EKE is similar. They are located in the area of the LV, as well as in the eastern part of the LB along the 1000 and 2000 m isobaths. A distinctive feature is the maxima of MLD in the western part of the LB near the slope of the Mohn Ridge, which is not accompanied by an increase in EKE. Note that such a discrepancy is also typical for the NB, where some

increase in MLD is not due to eddy activity.

In TOPO3, the maximum values of EKE as well as MLD shift to the central part of the NB, while the southern and eastern parts of the NB exhibit minimum values of EKE and MLD. It is worth noting that a significant increase in eddy activity in the eastern part of the LB near the continental slope of Norway does not lead to a similar increase in MLD. Moreover, in the TOPO3 experiment, as well as in TOPO2, the values of MLD are even lower here than in TOPO1, where the bottom topography corresponds to the real values. This may be because of slope convection, the conditions are more favorable when there is a gradual lowering of the bottom relief, rather than abrupt, as in TOPO2 and TOPO3. Changes in the topography of the continental slope contribute to an increase in EKE in the southern part of the Norwegian mainland slope, which, however, does not lead to an increase in MLD in this area. Such a decrease in eddy activity leads to a weakening of the process of intense deep convection and maximum convection in the LB in February in the TORO4 experiment does not exceed 325 m. Since the maxima of EKE are not observed in the area, the convection here is mainly slope type where the high values of MLD are confined to the isobaths, and they are not

connected with maxima of EKE.

## 4. Discussion and Conclusions

We analyzed a series of topographic experiments using a regional configuration of the MITgcm driven by the same lateral and surface boundary conditions, but with different bottom topography in the Norwegian Sea. Our main findings are: (1) A bowl-shaped bottom topography is a necessary condition for the formation of the Lofoten Vortex of the Norwegian Sea; (2) The existence of a boundary between the LB and NB (Helgeland Ridge) is crucial for the generation of the LV as eddies do not leave the LB for the adjacent NB. When the boundary between the basins is removed, a quasi-permanent anticyclonic vortex is formed in the NB.

As shown in the numerical experiments of *Shchepetkin* [1995], the existence of cyclonic circulation at the periphery of a rectangular idealized basin and the generation of an anticyclonic vortex in the center of this basin is due to bowl-shaped bottom topography. Our experiments confirmed this result. The quasi-permanent anticyclonic Lofoten Vortex is generated only then when the basin is bounded from all sides. Moreover, *Be-*

*nilov* [2005], using a two-layer quasi-geostrophic model, showed theoretically that the bottom topography in the form of a bowl determines the stability of this anticyclonic vortex which is generated in TOPO1 and TOPO2.

When the boundary between the basins is removed, the vortex does not form in the LB but it is generated in the NB instead. Mesoscale eddies generated mostly by the dynamic instability of the NwASC [*Köhl*, 2007; *Isachsen*, 2011, 2015; *Volkov et al.*, 2015] move west across the LB and reach the NB where the bowl-shaped bottom topography promotes the generation of an anticyclonic vortex in the NB (TOPO3). However, the generated vortex in the NB in the TOPO3 experiment is weaker than the LV in TOPO1 and TOPO2.

Another possible mechanism influencing the intensity and stability of the quasi-permanent anticyclonic vortex is the winter deep convection [*Alexeev et al.*, 2016; *Fedorov et al.*, 2019; *Søiland et al.*, 2016; *Travkin and Belonenko*, 2020]. The stabilization of the vortex is due to a periodic increase of the horizontal gradients of potential vorticity across its boundaries [*Bloshkina and Ivanov*, 2016; *Bashmachnikov et al.*, 2017a]. Thus, it is possible that the topography of the LB and NB is favorable for the development of convection in the

spring-winter period. The roughness of the seafloor in the NB hinders the intensity of convection (TOPO4), while a flat bottom in the LB with depths of more than 3000 m has a beneficial effect on the development of convection and the high values of MLD. It was found that MLD in the NB is much less than in the LB. Besides, the maximum development of dep convection for all TOPO experiments is most pronounced in February and somewhat weaker in March.

The spatial distribution of MLD indicates the development of the maximum intensity in the area where the LV is located which is shown in the TOPO1 and TOPO2 experiments. When the topography of the LB changes, the maximum convection areas shift either towards the western part of the LB and the Vøring Plateau and the mainland slope (TOPO4) or to the central part of the NB (TOPO3). The Vøring Plateau is characterized by high values of MLD, while the process of winter-spring convection in this area practically does not occur when the Vøring Plateau is removed from the bottom topography data (TOPO2 and TOPO3). Such an increase of MLD in the area of the Vøring Plateau is also described by *Nilsen and Falck* [2006] who explained the increase of MLD with an increased residence time of the Atlantic Waters in this

region due to divergence of the branches of the NwAC.

The topographical isolation of the LB and the presence of a decrease in the bottom relief in its central part leads there to the formation of EKE maxima in the central part of the LB and almost complete absence of eddy activity in the NB (TOPO1 and TOPO2). The winter convection is accompanied by intense horizontal eddy mixing on several scales. *Killworth* [1983] noticed that the winter convection with a horizontal scale of 1 km is accompanied by eddies of scales of 5 to 50 km. Our results fully support this idea.

**Acknowledgments.** The authors acknowledge the support of the Russian Science Foundation (RSF, project No. 18-17-00027). Numerical experiments were conducted by DLV with support from the NOAA Atlantic Oceanographic and Meteorological Laboratory under the auspices of the Cooperative Institute of Marine and Atmospheric Studies (CIMAS) of the University of Miami and NOAA, cooperative agreement NA20OAR4320472.

## Electronic Supplements

Seven electronic supplements (five videos and two figures) are published below.

Supplement **747-fra.mp4** (video)

- Supplement **747-s01.png** (figure)
- Supplement **747-s02.png** (figure)
- Supplement **747-t01.mp4** (video)
- Supplement **747-t02.mp4** (video)
- Supplement **747-t03.mp4** (video)
- Supplement **747-t04.mp4** (video)

## References

- Adcroft, A., C. Hill, J. Marshall (1997) , The representation of topography by shaved cells in a height coordinate model, *Mon. Weather Rev.*, 125, p. 2293–2315, [Crossref](#)
- Alexeev, V. A., V. V. Ivanov, I. A. Repina, et al. (2016) , Convective structures in the Lofoten Basin based on satellite and Argo data, *Izv. Atmos. Ocean. Phys.*, 52, no. 9, p. 1064–1077, [Crossref](#)
- Alekseev, G. V., M. V. Bagryantsev, P. V. Bogorodsky, et al. (1991) , Structure and circulation of waters in the North-East of the Norwegian sea, *Problems of the Arctic and Antarctic. Issue 65*, p. 14–23, Hydrometeoizdat, Leningrad.
- Bashmachnikov, I. L., T. V. Belonenko, P. A. Kuibin (2017a) , The application of the theory of the columnar Q-vortex with helical structure to the description of the dynamic characteristics of the Lofoten vortex of the Norwegian sea, *Vestn. St. Petersburg Un-ta Ser. 7*, 62, no. 3, p. 21–336, [Crossref](#)
- Bashmachnikov, I. L., et al. (2017b) , On the vertical structure

and stability of the Lofoten vortex in the Norwegian Sea, *Deep-Sea Res. I*, 128, p. 1–27, [Crossref](#)

Bashmachnikov, I., T. Belonenko, P. Kuibin, et al. (2018) , Pattern of vertical velocity in the Lofoten vortex (the Norwegian Sea), *Ocean Dynamics*, 68, no. 12, p. 1711–1725, [Crossref](#)

Belonenko, T. V., I. L. Bashmachnikov, et al. (2017) , On the Vertical Velocity Component in the Mesoscale Lofoten Vortex of the Norwegian Sea, *Izvestiya, Atmospheric and Oceanic Physics*, 53, no. 6, p. 641–649, [Crossref](#)

Belonenko, T. V., A. V. Koldunov, et al. (2018) , Thermohaline structure of the Lofoten vortex in the Norwegian sea based on field research and hydrodynamic modeling, *Vestn. S. Petersbur. Un-ta, Earth Sciences*, 63, no. 4, p. 502–519, [Crossref](#)

Belonenko, T. V., D. L. Volkov, et al. (2014) , Circulation of waters in the Lofoten Basin of the Norwegian Sea, *Vestn. S. Petersbur. Un-ta*, 7, no. 2, p. 108–121 (in Russian).

Belonenko, T., V. Zinchenko, et al. (2020) , Evaluation of Heat and Salt Transports by Mesoscale Eddies in the Lofoten Basin, *Russ. J. Earth Sci.*, 20, [Crossref](#)

Benilov, E. S. (2005) , Stability of a Two-Layer Quasigeostrophic Vortex over Axisymmetric Localized Topography, *J. Phys. Oceanogr.*, 35, no. 1, p. 123–130, [Crossref](#)

Bloshkina, E. V., V. V. Ivanov (2016) , Convective structures in the Norwegian and Greenland Seas based on simulation results with high spatial resolution, *Proceedings of the Hydrometeorological Research Center of the Russian Federation*, 361, p. 146–168 (in Russian).

Bosse, A., I. Fer, et al. (2019) , Dynamical controls on the

longevity of a non-linear vortex: The case of the Lofoten Basin Eddy, *Scientific Reports*, 9, no. 13,448, p. 1–13, [Crossref](#)

Carnevale, G. F., R. C. Kloosterziel, G. J. F. van Heijst (1991) , Propagation of barotropic vortices over topography in a rotating tank, *J. Fluid Mech.*, 233, p. 119–125, [Crossref](#)

Dugstad, J., I. Fer, J. LaCasce, et al. (2019) , Lateral heat transport in the Lofoten Basin: Near-surface pathways and subsurface exchange, *Journal of Geophysical Research: Oceans*, 124, p. 2992–3006, [Crossref](#)

Fedorov, A. M., I. L. Bashmachnikov, T. V. Belonenko (2018) , Localization of areas of deep convection in the Nordic seas, the Labrador Sea and the Irminger Sea, *Vestn. S. Petersbur. Un-ta, Earth Sciences*, 63, no. 3, p. 345–362, [Crossref](#)

Fedorov, A. M., I. L. Bashmachnikov, T. V. Belonenko (2019) , Winter convection in the Lofoten Basin according to ARGO buoys and hydrodynamic modeling, *Vestn. S. Petersbur. Un-ta, Earth Sciences*, 64, no. 3, p. 491–511, [Crossref](#)

Fer, I., A. Bosse, et al. (2018) , The Dissipation of Kinetic Energy in the Lofoten Basin Eddy, *Journal of Physical Oceanography*, 48, no. 6, p. 1299–1305, [Crossref](#)

Gascard, J.-C., K. A. Mork (2008) , Climatic importance of large-scale and mesoscale circulation in the Lofoten Basin deduced from Lagrangian observations Arctic-Subarctic Ocean Fluxes, *Defining the Role of the Northern Seas in Climate*, p. 131–144, Springer Science, [Crossref](#)

Gordeeva, S., V. Zinchenko, et al. (2020) , Statistical analysis of long-lived mesoscale eddies in the Lofoten Basin from satellite

altimetry, *Advances in Space Research*, [Crossref](#)

Isachsen, P. E. (2011) , Baroclinic instability and eddy tracer transport across sloping bottom topography: How well does a modified Eady model do in primitive equation simulations?, *Ocean Model.*, *39*, p. 183–199, [Crossref](#)

Isachsen, P. E. (2015) , Baroclinic instability and the mesoscale eddy field around the Lofoten Basin, *J. Geophys. Res.*, *120*, no. 4, p. 2884–2903, [Crossref](#)

Isachsen, P. E., J. H. LaCasce, et al. (2003) , Wind-driven variability of the large-scale recirculating flow in the Nordic seas and Arctic Ocean, *J. Phys. Oceanogr.*, *33*, p. 2534–2550, [Crossref](#)

Ivanov, V. V., A. A. Koralev (1995a) , Formation and regeneration of the pycnocline lens in the Norwegian Sea, *Russ. Meteor. Hydrol.*, *9*, p. 62–69.

Ivanov, V. V., A. A. Koralev (1995b) , Dynamics of an intrapycnocline lens in the Norwegian Sea, *Russ. Meteor. Hydrol.*, *10*, p. 32–37.

Jakobsen, P., M. Ribergaard, et al. (2003) , Near-surface circulation in the northern North Atlantic as inferred from Lagrangian drifters: Variability from the mesoscale to interannual, *Journal of Geophysical Research*, *108*, no. C8, p. 3251–3254, [Crossref](#)

Kara, A. B., P. A. Rochford, H. E. Hurlburt (2000) , An optimal definition for ocean mixed layer depth, *Journal of Geophysical Research*, *105*, no. C7, p. 16,803–16,821, [Crossref](#)

Killworth, P. D. (1983) , Deep convection in the World Ocean, *Reviews of Geophysics*, *21*, no. 1, p. 1, [Crossref](#)

Kohl, A. (2007) , Generation and Stability of a Quasi-Permanent Vortex in the Lofoten Basin, *J. Phys. Oceanogr.*, *37*, p. 2637–

2651, [Crossref](#)

Koszalka, I., J. H. LaCasce, M. Andersson, et al. (2011) , Surface circulation in the Nordic seas from clustered drifters, *Deep-Sea Res. I*, 58, p. 468–485, [Crossref](#)

Large, W. G., J. C. McWilliams, S. C. Doney (1994) , Oceanic vertical mixing: are view and a model with an on local boundary layer parameterization, *Rev. Geophys.*, 32, p. 363–403, [Crossref](#)

Losch, M., D. Menemenlis, et al. (2010) , On the formulation of sea-ice models. Part1: Effects of different solver implementations and parameterizations, *Ocean Model.*, 33, p. 129–144, [Crossref](#)

Marshall, J., A. Adcroft, C. Hill, et al. (1997) , A finite volume, incompressible Navier–Stokes model for studies of the ocean on parallel computers, *J. Geophys. Res.*, 102, p. 5753–5766, [Crossref](#)

Nguyen, A. T., D. Menemenlis, R. Kwok (2011) , Arctic ice-ocean simulation with optimized model parameters: approach and assessment, *J. Geophys. Res.*, 116, p. C04025, [Crossref](#)

Nilsen, J. E., E. Falck (2006) , Variations of mixed layer properties in the Norwegian Sea for the period 1948–1999, *Progress in Oceanography*, 70, p. 58–89, [Crossref](#)

Nost, O. A., P. E. Isachsen (2003) , The large-scale time-mean ocean circulation in the Nordic Seas and Arctic Ocean estimated from simplified dynamics, *Journal of Marine Research*, 61, p. 175–210, [Crossref](#)

Orvik, K. (2004) , The deepening of the Atlantic water in the Lofoten Basin of the Norwegian Sea, demonstrated by using an

active reduced gravity model, *Geophysical Research Letters*, 31, no. L01306, p. 1–3, [Crossref](#)

Orvik, K., P. P. Niiler (2002) , Major pathways of Atlantic water in the northern North Atlantic and Nordic seas toward Arctic, *Geophys. Res. Lett.*, 29, p. 1896, [Crossref](#)

Poulain, P.-M., A. Warn-Varnas, P. Niiler (1996) , Near surface circulation of the Nordic Seas as measured by lagrangian drifters, *Journal of Geophysical Research*, 101, no. C8, p. 18,237–18,258, [Crossref](#)

Raj, R. P., I. Halo (2016) , Monitoring the mesoscale eddies of the Lofoten Basin: importance, progress, and challenges, *International Journal of Remote Sensing*, 37, no. 16, p. 3712–3728, [Crossref](#)

Raj, R. P., I. Halo, S. Chatterjee, et al. (2020) , Interaction between mesoscale eddies and the gyre circulation in the Lofoten Basin, *JGR Oceans*, [Crossref](#)

Rossby, T., V. Ozhigin, et al. (2009) , An isopycnal view of the Nordic Seas hydrography with focus on properties of the Lofoten Basin, *Deep-Sea Research I*, 56, no. 11, p. 1955–1971, [Crossref](#)

Smith, W. H. F., D. T. Sandwell (1997) , Global sea floor topography from satellite altimetry and ship depth soundings, *Science*, 277, no. 5334, p. 1956–1962, [Crossref](#)

Soiland, H., L. Chafik, T. Rossby (2016) , On the long-term stability of the Lofoten Basin Eddy, *J. Geophys. Res. Oceans*, 121, p. 4438–4449, [Crossref](#)

Shchepetkin, A. F. (1995) , Interaction of turbulent barotropic shallow-water flow with topography, 1995, *Proceedings of Hawaii-*

ian Winter Aha Huliko'a Workshop, P. Müller and D. Henderson (eds), p. 225–237, HI, Honolulu.

Travkin, V. S., T. V. Belonenko (2020) , Mixed layer depth in winter convection in the Lofoten Basin in the Norwegian Sea and assessment methods. *Hydrometeorology and Ecology, Proceedings of the Russian State Hydrometeorological University*, 59, p. 67–83, [Crossref](#)

Voet, G., D. Quadfasel, et al. (2010) , The mid-depth circulation of the Nordic Seas derived from profiling float observations, *Tellus A*, 62, no. 4, p. 516–529, [Crossref](#)

Volkov, D. L., T. V. Belonenko, V. R. Foux (2013) , Puzzling over the dynamics of the Lofoten Basin – a sub-Arctic hot spot of ocean variability, *Geophys. Res. Lett.*, 40, no. 4, p. 738–743, [Crossref](#)

Volkov, D. L., A. A. Kubryakov, R. Lumpkin (2015) , Formation and variability of the Lofoten basin vortex in a high-resolution ocean model, *Deep-Sea Res. I*, 105, p. 142–157, [Crossref](#)

Yu, L.-S., A. Bosse, I. Fer, et al. (2017) , The Lofoten Basin eddy: Three years of evolution as observed by Seagliders, *Journal of Geophysical Research: Oceans*, 122, no. 8, p. 6814–6834, [Crossref](#)

Zinchenko, V. A., S. M. Gordeeva, et al. (2019) , Analysis of Mesoscale eddies in the Lofoten Basin based on satellite altimetry, *Fundamentalnaya i Prikladnaya Gidrofizika*, 12, no. 3, p. 46–54, [Crossref](#)

---